# Magnetically driven giant negative thermal expansion covering room temperature in Hf0.875Ta0×125Fe2

L. V. B. Diop, O. Isnard

# Magnetically driven giant negative thermal expansion covering room temperature in $Hf_{0.875}Ta_{0.125}Fe_2$

L.V.B. Diop[1,2*] and O. Isnard[2]

[1]Université de Lorraine, CNRS, IJL, F-54000 Nancy, France

[2]Université Grenoble Alpes, CNRS, Institut NEEL, F-38042 Grenoble, France

**ABSTRACT**

Neutron diffraction is used to reveal the origin of the unusual thermal expansion properties of the itinerant-electron system $Hf_{0.875}Ta_{0.125}Fe_2$. $Hf_{0.875}Ta_{0.125}Fe_2$ shows temperature-induced magnetic transitions from ferromagnetic (FM) to antiferromagnetic (AFM) order and then to the paramagnetic (PM) state upon heating. The FM-AFM transition proceeds in a stepwise fashion, as a first-order phase transition, and is accompanied by an extremely anisotropic lattice collapse. The unit cell volume shrinks abruptly, but only in the basal plane; the dimension along the *c*-axis varies almost continuously. $Hf_{0.875}Ta_{0.125}Fe_2$ exhibits a 0.37 % spontaneous volume contraction across the FM-AFM transition, where a giant negative thermal expansion (NTE), with a volumetric thermal expansion coefficient $-74\times10^{-6}$ $K^{-1}$, is observed over a temperature interval of $\Delta T\sim50$ K around room temperature.

**Keywords:** A. Intermetallic compound; C. Neutron powder diffraction; D. Negative thermal expansion; D. Magnetoelastic transition.

* E-mail address: leopold.diop@univ-lorraine.fr

## 1. Introduction

It is general knowledge that most materials expand when they are heated and contract upon cooling under constant pressure (positive thermal expansion, PTE). However, only a few materials behave inversely, i.e., shrink upon heating while expand upon cooling, which is called negative thermal expansion (NTE). Materials featuring the NTE properties are of great importance for both scientific research and modern technological applications[1-4]. NTE systems have enormous industrial merit because they can be used to tune and control the overall thermal expansion of materials. NTE materials are generally combined with usual PTE materials to fabricate the zero thermal expansion (ZTE) composites[5-11], which are desirable in many fields such as high-precision optics and aerospace[12-15]. NTE materials are mainly used as the thermal-expansion inhibitor for making the composites with precisely tailored coefficient of thermal expansion. Therefore, there are a number of important potential technical applications of NTE materials used as, for example, high-precision optical mirrors, optical fiber reflective grating devices, athermalizer for Bragg grating, printed circuit boards and machinery parts.

Up to the present time materials of various kinds have been identified and investigated for their potential as NTE materials. In addition to the well-studied $ZrW_2O_8$ family of materials[4], NTE effects have also been observed in silicates β-$LiAlSiO_4$[16], cyanides $Cd(CN)_2$[17], $ReO_3$[18], CuO nanoparticles[3], $ScF_3$[19-21], $PbTiO_3$-based ferroelectrics[22], antiperovskite manganese nitrides[23-24], and as well as reduced layered ruthenate $Ca_2RuO_{3.74}$[25]. Nevertheless, only a very limited number of NTE materials serve as high-performance thermal-expansion compensators, due to low coefficient of thermal expansion, the relatively narrow NTE temperature window, thermal expansion anisotropy, as well as low mechanical and/or electrical insulating properties. Traditional NTE systems with flexible framework in the crystal structure (e.g., $ZrW_2O_8$ and $ScF_3$) usually display NTE over a wide temperature range up to 1000 K, but the related coefficient of linear thermal expansion, $\alpha$, can hardly go beyond $-10\times10^{-6}$ $K^{-1}$. Unfortunately, their NTE coefficient, is so small that a large amount of addition is needed in order to obtain high-performance ZTE composites. In practical applications, a large coefficient of thermal expansion, which can effectively compensate the thermal expansion of PTE matrix but with little influence on its original physical properties, is thus desirable for NTE material.

Colossal NTE has been discovered during the last decade in various classes of materials, particularly systems associated with a metal-insulator [25,26], intermetallic charge-transfer[27,28] or ferroelectric transition[29]. Most recently, the utilization of a magnetic phase transition

accompanied by large volume reduction upon heating is deemed as a promising avenue towards discovery of giant NTE. The effectiveness of this approach was recognized widely by the giant NTE reported for the $Mn_3AN$-based antiperovskite manganese nitrides (*A*: the main group elements or 3*d* elements) which use volume change due to the magnetic transformation, i.e., magnetovolume effects. The giant NTE of the antiperovskite manganese nitrides strongly influenced subsequent research, leading to the discovery of many phase-transition-type NTE intermetallic systems such as $MnCo_{0.98}Cr_{0.02}Ge$[30] and $La(Fe,Si,Co)_{13}$[31], which exhibit large magnetovolume effects. For instance, a large coefficient of linear thermal expansion $\alpha = -26\times10^{-6}$ $K^{-1}$ was achieved in the itinerant-electron compound $LaFe_{10.5}CoSi_{1.5}$ by proper chemical doping in $La(Fe,Si)_{13}$-based alloys. In the magnetic systems, the magnetovolume effect may significantly influence the overall thermal expansion. A prominent example is the Invar alloys, which present very low PTE or NTE below the magnetic ordering Néel or Curie temperatures. The magnetic moment-volume instability was argued to cause NTE, which suppresses the usual PTE and consequently leads to the Invar effect. It is well established that the unit-cell volume of a ferromagnetic (FM) spin configuration is usually larger than that of an antiferromagnetic (AFM) one; hence giant NTE could be discovered at the FM-AFM magnetic transition.

To this end, one interesting example is the itinerant-electron system $Hf_{1-x}Ta_xFe_2$, when $0.1 < x < 0.3$. The alloys in this compositional range crystallize in the hexagonal $MgZn_2$-type structure (C-14 Laves phase, space group $P6_3/mmc$) in which the Fe atoms are located on two inequivalent Wyckoff positions (2a and 6h) with the Hf/Ta atoms occupying the 4f site. The compounds undergo a first-order ferromagnetic (FM) to antiferromagnetic (AFM) phase transition upon heating[32-35]. This FM-AFM first-order phase transition is critical for technological applications, as it is accompanied by strong responses to relatively minor stimuli, such as large magnetocaloric, magnetoresistive, magnetostrictive or external pressure effects. In the present work, we report giant room-temperature NTE in polycrystalline $Hf_{0.875}Ta_{0.125}Fe_2$, chosen in the most interesting part of the $(Hf,Ta)Fe_2$ magnetic phase diagram with coexistence of FM and AFM behavior. We investigate the magnetovolume effects, such as the spontaneous volume magnetostriction and the pressure effects, in correlation with magnetic properties due to the Fe sublattice. We report how first-order phase transition correlates to instabilities of magnetic structures in this itinerant-electron compound. To determine the spin configurations and understand their coupling with the lattice, we conducted a detailed high-intensity neutron powder diffraction study as a function of both temperature and applied pressure.

## 2. Methods

The alloy of composition $Hf_{0.875}Ta_{0.125}Fe_2$ was prepared by melting high-purity constituting metals (at least 99.95%) in a high frequency induction furnace under a purified atmosphere of argon. The sample was melted three times with the button flipped over after each melting, which is usually sufficient to achieve compositional homogeneity. The so-obtained ingot was wrapped in tantalum foil, sealed in an evacuated quartz tube and annealed in a resistive furnace as follows. It was heated up to 1000 °C at a rate of 5 °C/minute and kept at this temperature for one week. Then, the power was switched off and the furnace quickly cooled down to room temperature. Neutron powder diffraction (NPD) measurements were carried out at the Institut Laue Langevin (ILL) in Grenoble, France. About 3 g of powder were introduced into a cylindrical vanadium sample holder ($D$ = 6 mm, $H$ = 5 cm) and mounted on the stick of a He cryostat, whose contribution to the powder diffraction patterns was eliminated using a radial oscillating collimator. Several patterns were collected at selected temperatures ranging between 2 and 400 K on the high-intensity diffractometer D1B ($\lambda$ = 2.52 Å and $\lambda/2$ = 1.26 Å) with a detector angular range coverage $5° \leq 2\theta \leq 128°$ which is especially suited for magnetic structure determination. All measurements were performed upon heating after temperature stabilization with typical acquisition times of 20 minutes per isotherm. A second set of powder diffraction patterns was collected while ramping temperature at 1 K/minute. The Rietveld analysis was performed using the FullProf program[36], which allows the simultaneous refinement of structural and magnetic profiles. NPD spectra were also recorded under hydrostatic pressure up to 1 GPa on D1B instrument. The pressure cell was made of Ti-Zr alloys. In order to avoid diffraction from the cell itself a composition of $Ti_{0.525}Zr_{0.475}$ mass content was used enabling the compensation of the coherent scattering length $b_c$ of Ti and Zr ($b_c^{Ti} = -3.438$ fm, $b_c^{Zr} = 7.16$ fm). The aluminium container was filled with fluorinert F77 as a pressure transmitting medium.

## 3. Results and discussion

For a deeper insight into the peculiar behavior of this system, a precise knowledge of both crystallographic and magnetic structure is required. With that aim, we have carried out NPD studies to establish the magnetic structures of this compound and its temperature dependence. A detailed Rietveld analysis has been performed on diffraction patterns collected

at selected representative temperatures in the PM, AFM and FM states, in order to refine the crystal structure and magnetic ordering – Figs.1a-1c. The pattern recorded at 375 K (PM state) is characteristic of the nuclear Bragg scattering only and all the Bragg peaks could be identified to arise from the original C-14 Laves phase structure (space group $P6_3/mmc$) found at room temperature.

The analysis of the 2 K pattern reveals that the $MgZn_2$-type crystal structure is preserved down to 2 K; no additional reflections have been observed as compared to the pattern collected in the PM phase. $Hf_{0.875}Ta_{0.125}Fe_2$ shows a ferromagnetic ordering of Fe moments below 310 K. The contribution of the magnetic order to the diffraction pattern is most clearly reflected by the presence of magnetic scattering on several Bragg peaks such as (100), (101) and (002). The Fe magnetic moments have been refined independently for the two non-equivalent sites and lie within the *ab*-plane of the hexagonal lattice. At 2 K, the refined moments of Fe at the 2a and 6h positions amount to 1.23 and 1.36 $\mu_B$ respectively. They are converted to 2.66 $\mu_B$ for one chemical formula, a value very consistent with the spontaneous magnetization 2.82 $\mu_B$ at 4 K for $Hf_{0.875}Ta_{0.125}Fe_2$[33].

$Hf_{0.875}Ta_{0.125}Fe_2$ is antiferromagnetic only in a limited temperature interval between $T_{FM\text{-}AFM}$ = 310 K and $T_N$ = 334 K. Over the same temperature range, the patterns display the same Bragg reflections as that in the PM regime, no additional magnetic peaks are detected. The analysis of the position of the magnetic reflections reveals that the corresponding AFM structure is described by the magnetic propagation vector **k** = (0, 0, 0) meaning that the magnetic unit cell is the same as the crystallographic one. The best refinement at 320 K is achieved for a spin configuration in which Fe-6h magnetic moments align ferromagnetically within the same layer while the coupling between successive Fe-6h layers is antiferromagnetic. In this AFM structure, the determined moment for Fe-6h atoms at 320 K is around 0.62 $\mu_B$, the Fe-2a atoms carry no ordered magnetic moment. The magnetic structures of $Hf_{0.875}Ta_{0.125}Fe_2$ are similar to those established elsewhere for neighbouring $Hf_{0.825}Ta_{0.175}Fe_2$ composition[37].

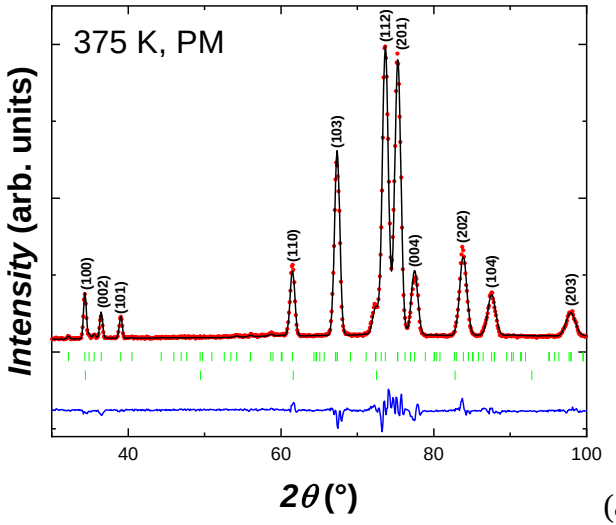


(a)

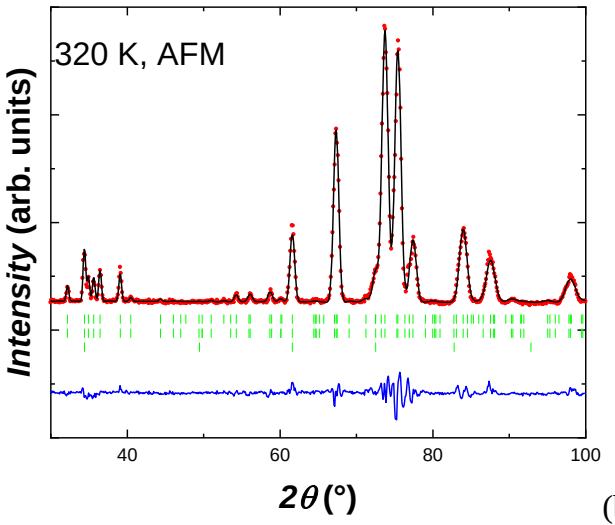


(b)

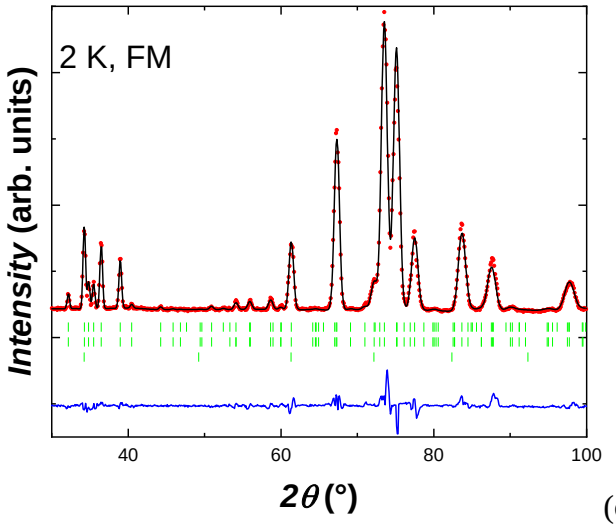


(c)

FIG. 1. Refinements of the neutron diffraction patterns recorded for $Hf_{0.875}Ta_{0.125}Fe_2$ at 375 K (a), 320 K (b) and 2 K (c). In the 375 K pattern, the top row of Bragg markers is for the $Hf_{0.875}Ta_{0.125}Fe_2$ nuclear contributions, the second row corresponds to the position of the vanadium sample environment contribution. At 2 and 320 K the top and second rows of Bragg markers are referring to the nuclear and magnetic contributions of the $Hf_{0.875}Ta_{0.125}Fe_2$ phase. The third row is corresponding to the nuclear contribution from the vanadium sample environment.

The thermal dependencies of the lattice parameters *a* and *c*, and the unit-cell volume *V* are displayed in Fig.2 and Fig.3, respectively. Below $T_{FM\text{-}AFM}$, *a* cell parameter stays nearly constant, while *c* gradually decreases upon cooling. At $T_{FM\text{-}AFM}$, the *a* lattice constant exhibits a large drop $\Delta a/a \approx 0.27$ % and the system gets transformed into the AFM state. On the contrary, *c* shows only a tiny change at $T_{FM\text{-}AFM}$. The first-order nature of the magnetic transition is reflected in the steep decrease of *a* parameter rather than the small anomaly in *c* lattice constant. It can be clearly seen that there exists a temperature range in which the cell dimensions in the basal plane expand with decreasing temperature. This signals a strong negative thermal expansion, leading to the linear thermal expansion coefficient $\alpha = (1/a)(\Delta a/\Delta T) = -54\times10^{-6}$ $K^{-1}$ over a temperature window of 50 K. This value is one order of magnitude larger than that for commercial NTE materials. [Typically, $\alpha$ is of the order of $10^{-6}$ $K^{-1}$, although for $ZrW_2O_8$, $\alpha = -9\times10^{-6}$ $K^{-1}$ (Ref. 16).] The first-order FM-AFM magnetic phase transition is accompanied with a significant spontaneous volume magnetostriction $\Delta V/V \approx 0.37$ %. This large magnetovolume effect is due to the abrupt change in the local magnetic moment, i.e., the amplitude difference of the Fe magnetic moment between the FM and AFM state. One can observe a peculiarly anisotropic character of the volume collapse at the magnetic transformation: the lattice shrinks suddenly, but only in the basal plane. The dimension along *c*-axis varies almost continuously across the transition.

The 0.37% volume drop occurs over a temperature interval of $\Delta T \sim 50$ K; the unit-cell volume shows a prominent NTE effect over this temperature span. It clearly indicates that the lattice expansion induced by the magnetic transition is larger than the thermal contraction due to the temperature decrease. Based on the refined values, we calculated the volume (bulk) thermal expansion coefficient $\beta = (1/V)(\Delta V/\Delta T)$ and the corresponding value is $\beta = -74\times10^{-6}$ $K^{-1}$. In the here studied compound, the volumetric thermal expansion coefficient is at least an order of magnitude larger than the value found in isostructural system $(Hf,Nb)Fe_2$[38,39] and $(Hf,Ti)Fe_2$[40]. Such a high NTE performance is also comparable to those of reported itinerant-electron intermetallic NTE materials: in $LaFe_{10.5}CoSi_{1.5}$ $\beta = -78\times10^{-6}$ $K^{-1}$ (Ref. 31).

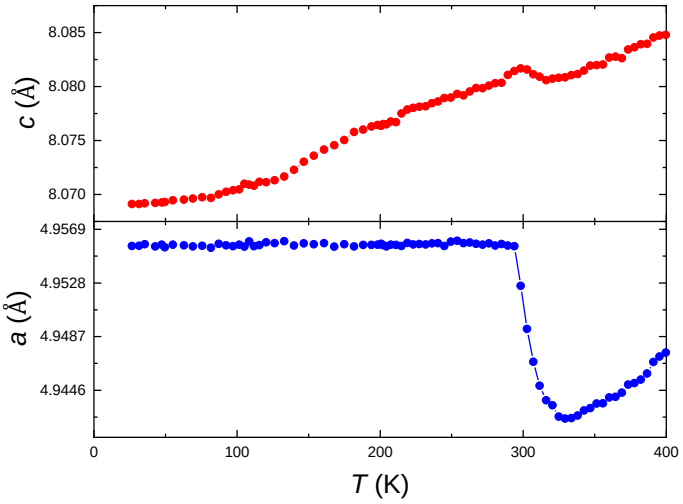


FIG. 2. Temperature dependence of the lattice parameters.

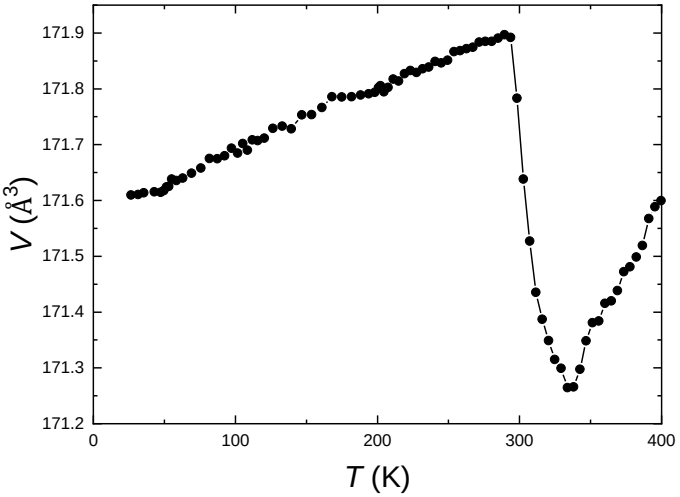


FIG. 3. Temperature dependence of the unit-cell volume.

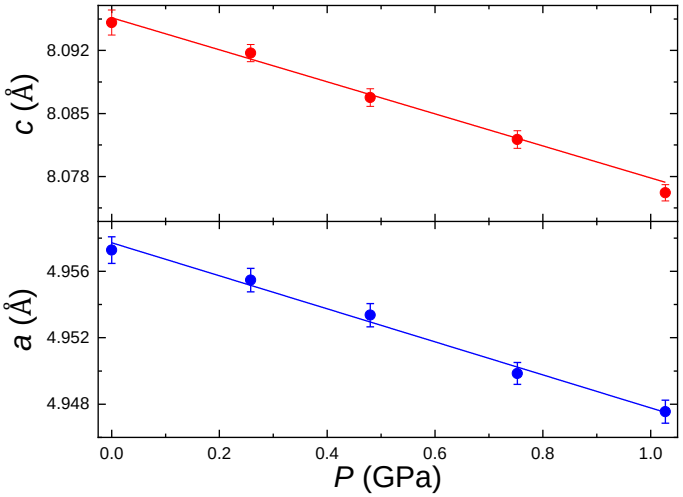


FIG. 4. Lattice parameters as a function of applied pressure.

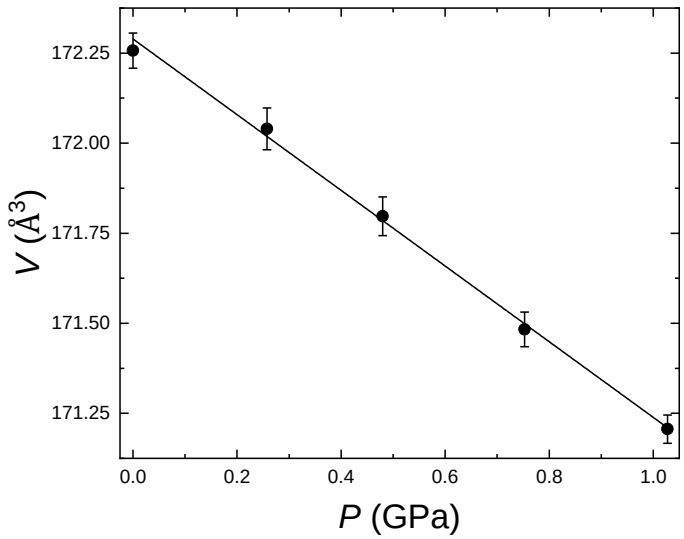


FIG. 5. Unit-cell volume as a function of applied pressure.

Because of the observed intimate relation between the crystal structure and the magnetic behavior in this itinerant-electron system, the application of hydrostatic pressure, thus changing the interatomic distances, should modify the transition temperatures, stabilizing the low-volume AFM phase. To probe the pressure dependence of the hexagonal lattice, NPD spectra have been collected up to 1 GPa at room temperature. NPD patterns recorded under pressures reveal that the hexagonal symmetry of the atomic arrangement remains unaltered within the investigated compression range; no indication of a structural phase transition was found up to the highest applied pressure. The lattice constants decrease linearly with pressure (Fig. 4), and values of d$a$/d$P$ = -10.1×10$^{-3}$ Å GPa$^{-1}$ and d$c$/d$P$ = -17.0×10$^{-3}$ Å GPa$^{-1}$ are obtained. The contraction of the hexagonal lattice is anisotropic and more pronounced along the $c$ direction whereas this lattice parameter was much less sensitive to the magnetic ordering temperature. The pressure dependence of the unit-cell volume is illustrated in Fig.5. The pressure induced decrease of the volume is linear with a slope of d$V$/d$P$ = -10.6×10$^{-1}$ Å$^3$ GPa$^{-1}$, leading to a compressibility value of $\kappa$ = 0.62×10$^{-2}$ GPa$^{-1}$. The obtained value compares very well with the compressibility for neighbouring $Hf_{0.825}Ta_{0.175}Fe_2$ composition ($\kappa$ = 0.57×10$^{-2}$ GPa$^{-1}$ Ref. 37).

## 4. Conclusion

In summary, the results presented here elucidate how NTE for the itinerant-electron system $Hf_{0.875}Ta_{0.125}Fe_2$ is intimately correlated with the magnetic structure. NPD studies

explained the underlying phenomena responsible for the giant NTE observed over a 50 K temperature interval – volumetric thermal expansion coefficient $-74\times10^{-6}$ $K^{-1}$. It is shown that this unusually large NTE is induced by the magnetoelastic transition from FM to AFM states. This FM-AFM transition is of first order and is accompanied by a stepwise drop of the magnetic moment and by an isomorphic lattice collapse of a peculiar anisotropic kind. The results unambiguously demonstrate that the disappearance of the magnetic moment of the Fe atoms at the 2a site plays a crucial role in the NTE of this system and sheds light on searching for NTE materials by tuning the competing magnetic orders.


## Acknowledgements

The authors gratefully acknowledge the Institut Laue Langevin for access to the neutron facility.


## References


[1]A.D. Fortes, E. Suard, and K.S. Knight, Science **331**, 742 (2011).

[2]Y.W. Long, N. Hayashi, T. Saito, M. Azuma, S. Muranaka, and Y. Shimakawa, Nature **458**, 60 (2009).

[3]X.G. Zheng, H. Kubozono, H. Yamada, K. Kato, Y. Ishiwata, and C.N. Xu, Nature Nanotechnol. **3**, 724 (2008).

[4]T.A. Mary, J.S.O. Evans, T. Vogt, and A.W. Sleight, Science **272**, 90 (1996).

[5]J. Chen, X.R. Xing, C. Sun, P.G. Hu, R.B. Yu, X.W. Wang, and L.H. Li, J. Am. Chem. Soc. **130**, 1144 (2008).

[6]I. Yanase, M. Miyagi, and H. Kobayashi, J. Eur. Ceram. Soc. **29**, 3129 (2009).

[7]K. Takenaka, and M. Ichigo, Compos. Sci. Technol. **104**, 47 (2014).

[8]R.J. Huang, Z. Chen, X.X. Chu, Z.X. Wu, and L.F. Li, J. Compos. Mater. **45**, 1675 (2011).

[9]K. Takenaka, Sci. Technol. Adv. Mater. **13**, 013001 (2012).

[10]L.M. Sullivan, and C. M. Lukehart, Chem. Mater. **17**, 2136 (2005).

[11]K. Takenaka, T. Hamada, D. Kasugai, and N. Sugimoto, J. Appl. Phys. **112**, 083517 (2012).

[12]K. Kintaka, J. Nishii, Y. Kawamoto, A. Sakamoto, and P. G. Kazansky, Opt. Lett. **27**, 1394 (2002).

[13]A. Sakamoto, T. Matano, and H. Takeuchi, IEICE Trans. Electron. **E83C**, 1441 (2000).

[14]J. Chen, L. Hu, J. X. Deng, and X.R. Xing, Chem. Soc. Rev. **44**, 3522 (2015).

[15]C.P. Romao, K.J. Miller, C.A. Whitman, M.A. White, and B.A. Marinkovic, *Negative Thermal Expansion (Thermomiotic) Materials* (Elsevier, Amsterdam, 2013).

[16]A.W. Sleight, Inorg. Chem. **37**, 2854 (1998).

[17]A.E. Phillips, A.L. Goodwin , G.J. Halder, P.D. Southon, and C.J. Kepert, Angew. Chem. Int. Ed. **47**, 1396 (2008).

[18]T. Chatterji, T.C. Hansen, M. Brunelli, and P.F. Henry, Appl. Phys. Lett. **94**, 241902 (2009).

[19]C.W. Li, X. Tang, J.A. Muñoz, J.B. Keith, S.J. Tracy, D.L. Abernathy, and B. Fultz, Phys. Rev. Lett. **107**, 195504 (2011).

[20]B.K. Greve, K.L. Martin, P.L. Lee, P.J. Chupas, K.W. Chapman, and A.P.Wilkinson, J. Am. Chem. Soc. **132**, 15496 (2010).

[21]J.P. Attfield, Nature **480**, 465 (2011).

[22]J. Chen, K. Nittala, J.S. Forrester, J.L. Jones, J. Deng, R. Yu, and X. Xing, J. Am. Chem. Soc. **133**, 11114 (2011).

[23]X. Song, Z. Sun, Q. Huang, M. Rettenmayr, X. Liu, M. Seyring, G. Li, G. Rao, and F. Yin, Adv. Mater. **23**, 4690 (2011)

[24]K. Takenaka, M. Ichigo, T. Hamada, A. Ozawa, T. Shibayama, T. Inagaki, and K. Asano, Sci. Technol. Adv. Mater. **15**, 015009 (2014).

[25]K. Takenaka, Y. Okamoto, T Shinoda, N. Katayama, and Y. Sakai, Nature Commun. **8**, 14102 (2017).

[26]M. Braden, G. André, S. Nakatsuji, and Y. Maeno Phys. Rev. B **58**, 847 (1998).

[27]M. Azuma, W. Chen, H. Seki, M. Czapski, S. Olga, K. Oka, M. Mizumaki, T. Watanuki, N. Ishimatsu, N. Kawamura, S. Ishiwata, M.G. Tucker, Y. Shimakawa, and J.P. Attfield, Nature Commun. **2**, 347 (2011).

[28]I. Yamada, K. Tsuchida, K. Ohgushi, N. Hayashi, J. Kim, N. Tsuji,R. Takahashi, M. Matsushita, N. Nishiyama, T. Inoue, T. Irifune, K. Kato, M. Takata, and M. Takano, Angew Chem. Int. Ed. **50**, 6579 (2011).

[29]J. Chen, X.R. Xing, G.R. Liu, J.H. Li, and Y.T. Liu, Appl. Phys. Lett. **89**, 101914 (2006).

[30]Y.Y. Zhao, F.X. Hu, L.F. Bao, J. Wang, H. Wu, Q.Z. Huang, R.R. Wu, Y. Liu, F.R. Shen, H. Kuang, M. Zhang, W.L. Zuo, X.Q. Zheng, J.R. Sun, and B.G. Shen, J. Am. Chem. Soc. **137**, 1746 (2015).

[31]R. Huang, Y. Liu, W. Fan, J. Tan, F. Xiao, L. Qian, and L. Li, J. Am. Chem. Soc. **135**, 11469 (2013).

[32]Y. Nishihara, and Y. Yamaguchi, J. Phys. Soc. Jpn. **52**, 3630 (1983).

[33]L.V.B. Diop, J. Kastil, O. Isnard, Z. Arnold, and J. Kamarad, J. Appl. Phys. **116**, 163907 (2014).

[34]P. Bag, R. Rawat, P. Chaddah, P.D. Babu, and V. Siruguri, Phys. Rev. B 93 014416, (2016).

[35]B. Li, X.H. Luo, H. Wang, W.J. Ren, S. Yano, C.W. Wang, J.S. Gardner, K.D. Liss, P. Miao, S.H. Lee, T. Kamiyama, R.Q. Wu, Y. Kawakita, and Z.D. Zhang, Phys. Rev. B **93**, 224405 (2016).

[36]J. Rodrıguez-Carvajal, Physica B **192**, 55 (1993).

[37]L.V.B. Diop, O. Isnard, E. Suard, and D. Benea, Solid. State Commun. **229**, 16 (2016).

[38]H. Yibole, A.K. Pathak, Y. Mudryk, F. Guillou, N. Zarkevich, S. Gupta, V. Balema, and V.K. Pecharsky, Acta Materialia **154**, 365 (2018).

[39]Y. Song, J. Chen, X. Liu, C. Wang, Q. Gao, Q. Li, L. Hu, J. Zhang, S. Zhang, and X. Xing, Chem. Mater. **29**, 7078 (2017).

[40]Y. Qiao, Y. Song, K. Lin, X. Liu, A. Franz, Y. Ren, J. Deng, R. Huang, L. Li, J. Chen, and X. Xing, Inorg. Chem. **58**, 5380 (2019).